

Magnetic Resonance Imaging and Cross-Sectional Anatomy of the Eye and the Optic Nerve in the Egyptian Donkey (*Equus asinus*)

Ashraf S Awaad^{1*}, Fatma M Halfaya², Azza A H Ibrahim¹ and Mohamed K M Abdel Maksoud¹

¹Anatomy and Embryology Department, Faculty of Veterinary Medicine, Beni-Suef University, Beni-Suef 62511, Egypt

²Surgery, Anesthesiology and Radiology Department, Faculty of Veterinary Medicine, Beni-Suef University, Beni-Suef 62511, Egypt

*Corresponding author: awaad2000@gmail.com

Article History: 21-414

Received: 04-Oct-21

Revised: 25-Nov-21

Accepted: 30-Nov-21

ABSTRACT

The eye is a high sense organ which is susceptible to many infectious and traumatic diseases. Using an accurate diagnostic imaging technique became essential for early detection and control of these diseases. The current investigation is proposed to fully describe the normal magnetic resonance imaging (MRI) appearance of the eye, extraocular structures and the optic nerve in the donkey with the aid of the anatomical sections. Eight fresh cadaveric heads of adult donkeys of both sexes were used; two were scanned using an MRI scanner of 1.5 Tesla magnet, and six were frozen to be sectioned into transverse (n=3) and frontal (n=3) sections. The accessed MR images were serially selected in matching to their corresponding gross sections. These MR images provided a comprehensive assessment of the eyeball structures (choroid, ciliary body, iris, cornea, sclera, anterior and posterior chambers, and vitreous body), the ocular adnexa (upper, lower and third eyelids, lacrimal gland, tarsal gland, superficial gland of the third eyelid, extraocular muscles and orbital fat), the various parts of the optic nerve (intraocular, intraorbital, intracanalicular, intracranial) and its surrounding meningeal sheath complex. However, it was difficult to outline the retina. The current investigation administrated a precise anatomical atlas of the eye, periorbital structures and optic nerve in the donkey assisting in the interpretation and diagnosis of both ocular diseases and optic neuropathy.

Key words: Anatomy, Donkey, Eye, Magnetic resonance imaging (MRI), Optic nerve.

INTRODUCTION

The donkeys are members of the family Equidae counting 43.5 million worldwide (FAO 2009). In third world countries, these animals are important for farming and transportation, but they were given less medical care and attention than other domestic animals (Salavati et al. 2017). In Egypt, the donkeys are essential farming animals due to their great tolerance (Amin et al. 2014).

The vision depends on a complex system including the eyeball and its accessory structures, optic nerve, and the visual area of the brain. The eye globe consists of three tunics; fibrous (cornea and sclera), vascular (choroid, ciliary body, iris) and nervous (retina). Moreover, the eyeball includes three chambers; anterior, posterior and vitreous. In addition, the ocular accessory structures include; the orbital fascia and fat, extraocular muscles and lacrimal apparatus (Konig and Liebich 2009). The optic nerve originates from the axons of the ganglionic nerve cells in the retina. Both optic nerves emerging from the

orbital cavity passing through the optic canals to decussate in the optic chiasma (Evans and de Lahunta 2013).

The common causes of the orbital diseases could be inflammatory, infectious, cystic, traumatic, or neoplastic (Grahn et al. 1993; Dennis 2000; Nell 2008; Van der Woerd 2008). It is necessary to promote an advanced imaging technique for the diagnosis and prognosis of these diseases (Hande and Talwar 2012). Recent diagnostic modalities for orbital imaging include radiography, computed tomography (CT), ultrasonography and magnetic resonance imaging (Penninck et al. 2001). Traditional radiography is an inadequate technique for imaging the eye globe soft tissues due to its unclear resolution as well as superimposition of the bony structures (Solano and Brawer 2004). Ultrasonography remains a rapid and feasible technique that is widely used for diagnosis of the ocular structures (Hallowell and Bowen 2007; Aironi and Gandage 2009; Laus et al. 2014; Gialletti et al 2018; Athar et al. 2021). However, using of ultrasonography for orbital imaging is limited due to its

Cite This Article as: Awaad AS, Halfaya FM, Ibrahim AAH and Maksoud MKA, 2022. Magnetic resonance imaging and cross-sectional anatomy of the eye and the optic nerve in the Egyptian donkey (*Equus asinus*). International Journal of Veterinary Science 11(4): 526-532. <https://doi.org/10.47278/journal.ijvs/2022.141>

inefficiency to visualize the orbital bony rim, the orbital apex and the intracranial extension of several ocular pathologies (Mafee 2003; Hande and Talwar 2012). Among imaging modalities CT and MRI are used extensively for evaluation of the eye globe (Goh et al 2008; Armour et al. 2011; D'Aout et al. 2014). CT is characterized by spatial resolution and discrimination between soft and bony tissue structures (D'Aout et al. 2014; Seddek et al. 2014; Awaad et al. 2019). However, MRI has priority in soft tissue visualization (Boroffka et al. 2007; Thrall 2013; Abdel Maksoud 2020, 2021; Abdel Maksoud et al. 2021). In addition, High-resolution MRI is recently used for the determination of the surgical interference in several ocular diseases (Kato et al. 2005; Maiolo et al. 2017).

The previous normal CT and MRI studies focused on the orbit and retrobulbar structures in the horse (Morgan et al. 1993; D'Aout et al. 2014), bovine (Litwiller et al. 2010), goat (Madkour et al. 2016) and dog and cat (Grahm et al. 1993; Morgan et al. 1994; Boroffka and Voorhout 1999; Boroffka et al. 2008; Armour et al. 2011). However, scarce studies intended to describe the normal eye structure of the eye with the aid of MRI in the donkey. The current study is proposed to describe briefly the normal MRI of the eye and the optic nerve in the donkey with the help of the cross anatomical sections.

MATERIALS AND METHODS

Ethical Statement

All procedures achieved in this investigation followed the guidelines of the Institutional Animal Care and Use Committee of Beni-Suef University, Egypt.

Animals

Eight heads from adult healthy donkeys (7-20 years old) of both sexes were used after euthanasia for reasons unrelated to ocular diseases or head injuries.

Magnetic Resonance Imaging

Two heads were examined by MRI within two hours from euthanasia. Using the human knee coil, the heads were placed with their longitudinal axis parallel to the examination table. Using a multi-planar MRI of 1.5 Tesla magnet (Philips Intera, Holland), T1-weighted (TR (repetition time) = 540 msec; TE (echo delay time) = 150 msec; FOV (field of view) = 21×21; Acq. Tm (acquisition time) = 21:18 min:s; slice thickness = 3.5mm; interstice space = 1mm) and T2-weighted (TR (repetition time) = 4073 msec; TE (echo delay time) = 100 msec; FOV (field of view) = 24×24; Acq. Tm (acquisition time) = 21:20 min:s; slice thickness = 3.5mm; interstice space = 1mm) spin-echo images were acquired. An automatic 3D reconstruction was used for the visualization of MR images in two planes; transverse and frontal. Graphical software (eFilm Workstation™ Merge Healthcare, Washington, USA) was used for manual reconstruction of the MR images.

Preparation of the Anatomical Sections

Six heads were frozen for seven days and then sectioned into transverse (n=3) and frontal (n=3) slices (1cm thickness) using a thin electrical band. These

anatomical sections were photographed using a digital camera (Samsung WB30F). These sections were grossly identified to be serially selected in matching with their corresponding MR images. The anatomical terms in the current study were in accordance with *Nomina Anatomica Veterinaria* (2017).

RESULTS

For comprehensive visualization and evaluation of the eyeball, retrobulbar structures, optic nerve and bony wall of the orbit, seven MR images were selected; three in transverse planes (Figs. 2-4) and four in frontal planes (Figs. 5-8). These planes were selected in matching to the reference lines designated along with the lateral aspect of the head region (Fig. 1).

The Eyeball

The eyeball was related topographically to the paranasal sinuses which were clearly depicted on MR images as hypointense structures on T1- and T2-weighted MR images. The frontal sinus was located dorsomedial to the orbit (Figs. 2-4, 6/fs) and the caudal maxillary sinus was found rostroventral to the orbit (Figs. 2, 5-7/ms). Moreover, the ethmoidal labyrinth appeared with heterogeneous intensity on both sequences of MRI and was positioned medial to the orbit (Figs. 2-8/el).

The eyeball was identified and evaluated with variable intensities on both T1- and T2- weighted MRI. The fluid chambers of the eye (anterior, posterior and vitreous) were depicted in transverse and frontal planes. These chambers appeared black (hypointense) on T1-weighted images (Figs. 5/ac, pc & 5, 7, 8/vc) and white (hyperintense) on T2-weighted images (Figs. 2, 3, 6/ac, pc, vc). The eye lens was located between the posterior chamber and vitreous body, and it appeared black (hypointense) on both sequences of MRI (Figs. 2, 3, 5/le). This lens was surrounded by a capsule which could be depicted only on T1-weighted images as a whitish (hyperintense) line surrounding the lens (Fig. 5/lec).

The anterior chamber was bounded rostrally by the cornea which constituted the rostral portion of the fibrous tunic and could be delineated on T1-weighted images with intermediate signal intensity (Fig. 5/co). While on T2-weighted images, the cornea appeared black (hypointense) and couldn't be distinguished from the surrounding black background (Figs. 2, 6/co). The caudal segment of the fibrous tunic, the sclera, appeared black (hypointense) on T1-weighted images (Figs. 5, 7/sc) and with intermediate signal intensity on T2-weighted images (Figs. 2-4, 6/sc).

The choroid was a thin layer and could be depicted with intermediate signal intensity on T1-weighted images (Fig. 5/cr) and black (hypointense) on T2-weighted images (Figs. 2-4, 6/cr). Both iris and ciliary body could be visualized with intermediate signal intensity on T1-weighted images (Fig. 5/cb, ir) and hypointense on T2-weighted images (Figs. 2, 6/cb, ir). However, the retina was difficult to be delineated on both MRI sequences.

Adnexa of the Eye

The orbital fat surrounding the eyeball and the ocular muscles appeared black (hypointense) on T1-weighted

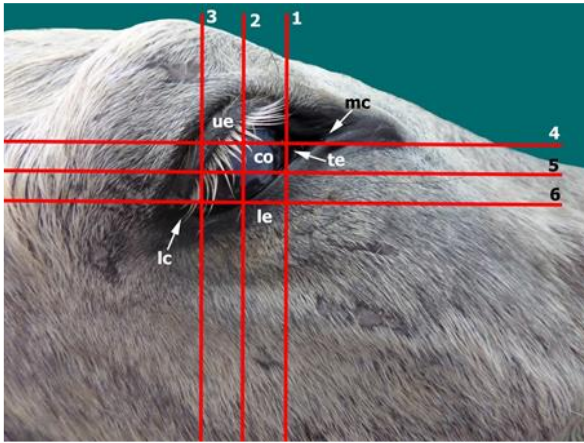


Fig. 1: Lateral aspect of the donkey face. The numbered red lines indicated the matched planes of each anatomical section with its compared magnetic resonance image; selected transverse planes (1-3) and frontal planes (4-6).

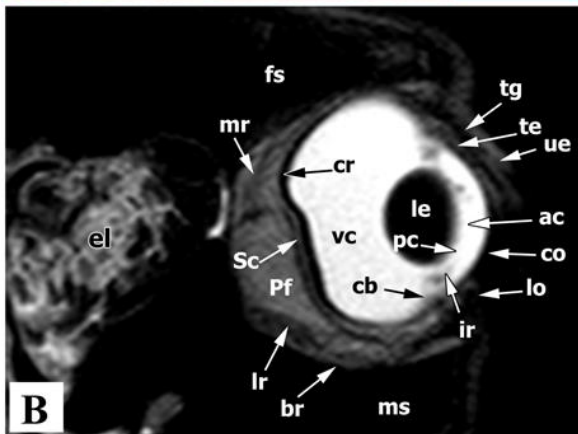
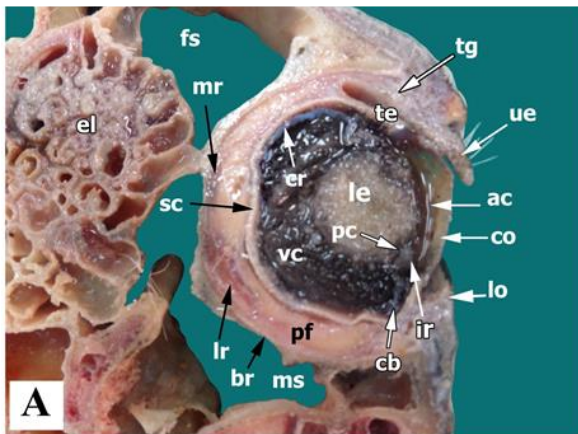


Fig. 2: Transverse sections of the left eye of the donkey (plane 1 as designated in Figure 1): anatomical section (A) and T2-wighted magnetic resonance image (B). ac- anterior chamber, br- bony rim, cb- ciliary body, co- cornea, cr- choroid, el- ethmoidal labyrinth, fs- frontal sinus, ir- iris, le- lens, lo- lower eyelid, lr- lateral rectus muscle, mr- medial rectus muscle, ms- maxillary sinus, pc- posterior chamber, pf- orbital fat, sc- sclera, te- third eyelid, tg- tarsal gland, ue- upper eyelid, vc- vitreous chamber.

images (Figs. 5, 7, 8/pf) and white (hyperintense) on T2-weighted images (Figs. 2-4, 6/pf). While the orbital fibroelastic sheath that encircled the optic nerve and all orbital contents couldn't be identified on both sequences of MRI.

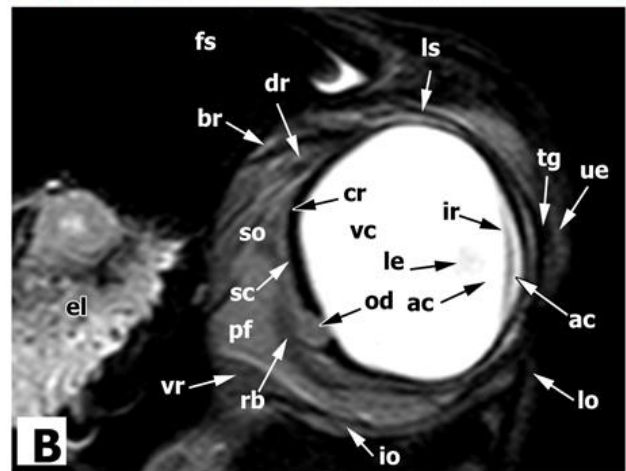
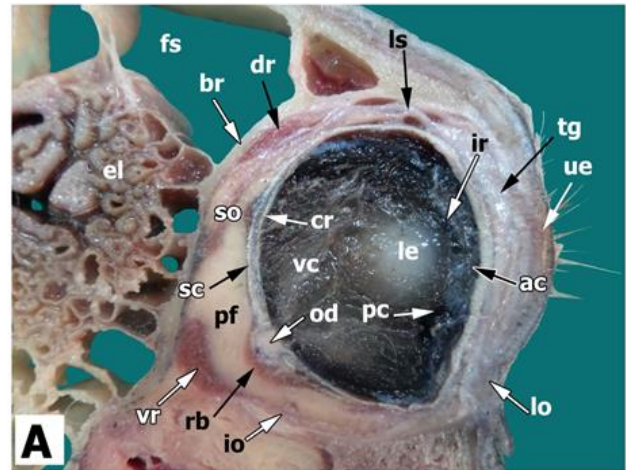


Fig. 3: Transverse sections of the left eye of the donkey (plane 2 as designated in Figure 1): anatomical section (A) and T2-wighted magnetic resonance image (B). ac- anterior chamber, br- bony rim, cr- choroid, dr- dorsal rectus muscle, el- ethmoidal labyrinth, fs- frontal sinus, io- inferior oblique muscle, ir- iris, le- lens, lo- lower eyelid, ls- levator palpebrae superioris muscle, od- optic disc, pc- posterior chamber, pf- orbital fat, rb- retractor bulbi muscle, sc- sclera, so- superior oblique muscle, tg- tarsal gland, ue- upper eyelid, vc- vitreous chamber, vr- ventral rectus muscle.

The eyelids were clearly delineated on the transverse and frontal planes of both sequences. The upper and lower eyelids were identified with intermediate signal intensity on T1-weighted images (Fig. 5/lo, ue) and low signal intensity on T2-weighted images (Figs. 2, 3, 6/lo, ue). Moreover, the third eyelid was positioned at the medial canthus of the eye and could be recognized on transverse and frontal planes with intermediate signal intensity on T1-weighted images (Fig. 5/te) and low signal intensity on T2-weighted images (Fig. 2/te).

The lacrimal gland was a lobulated structure found dorsolateral to the eye globe and on the ventromedial aspect of the zygomatic process of the frontal bone. The tarsal gland and superficial gland of the third eyelid were positioned within the free margin of the upper eyelid, and within the third eyelid respectively. These lacrimal glands appeared white (hyperintense) on T1-weighted images (Figs. 5, 7/lg & 5/sg, tg) and homogenous intense lobulated structures on T2-weighted images (Figs. 4, 6/lg & 6/sg & 2, 3/tg).

The extraocular muscles were clearly depicted on both MRI sequences with intermediate signal intensity. The medial lateral rectus, ventral rectus and the retractor bulbi

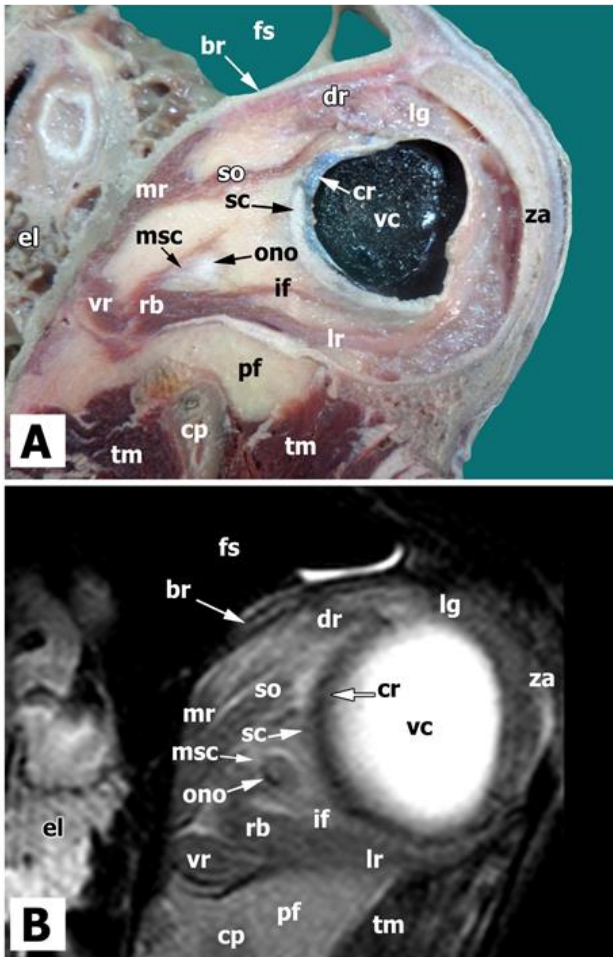


Fig. 4: Transverse sections of the left eye of the donkey (plane 3 as designated in Figure 1): anatomical section (A) and T2-weighted magnetic resonance image (B). br- bony rim, cr- choroid, cp- coronoid process of the mandible, dr- dorsal rectus muscle, el- ethmoidal labyrinth, fs- frontal sinus, if- inferior oblique muscle, lg- lacrimal gland, lr- lateral rectus muscle, mr- medial rectus muscle, msc- meningeal sheath complex, ono- intraorbital part of the optic nerve, pf- orbital fat, rb- retractor bulbi muscle, sc- sclera, so- superior oblique muscle, tm- temporal muscle, vc- vitreous chamber, vr- ventral rectus muscle, za- zygomatic arch.

muscles were best evaluated on both transverse and frontal planes (Figs. 4-7/mr, lr, rb & 3, 4, 6, 7/vr). While the dorsal rectus, two oblique muscles (superior and inferior) were best delineated on the transverse planes (Figs. 3, 6/dr, so & 4/if). Moreover, the levator palpebrae superioris muscle was best identified within the upper eyelid on the transverse plane (Fig. 3/lr). However, the orbicularis oris muscle couldn't be determined.

Optic Nerve

The optic nerve could be classified into four parts; intraocular, intraorbital, intracanalicular and intracranial. The former part originated from the retina in the form of an optic disc which was seen with intermediate signal intensity on both MRI sequences (Figs. 3, 7/od). The intraorbital part, passed caudoventrally between the retractor bulbi muscle fibers to reach the apex of the orbit, and it was referred on both MRI sequences as an intermediate signal intense structure (Figs. 4, 7, 8/ono). This part was surrounded by the cerebrospinal fluid within the meningeal sheath forming the meningeal sheath

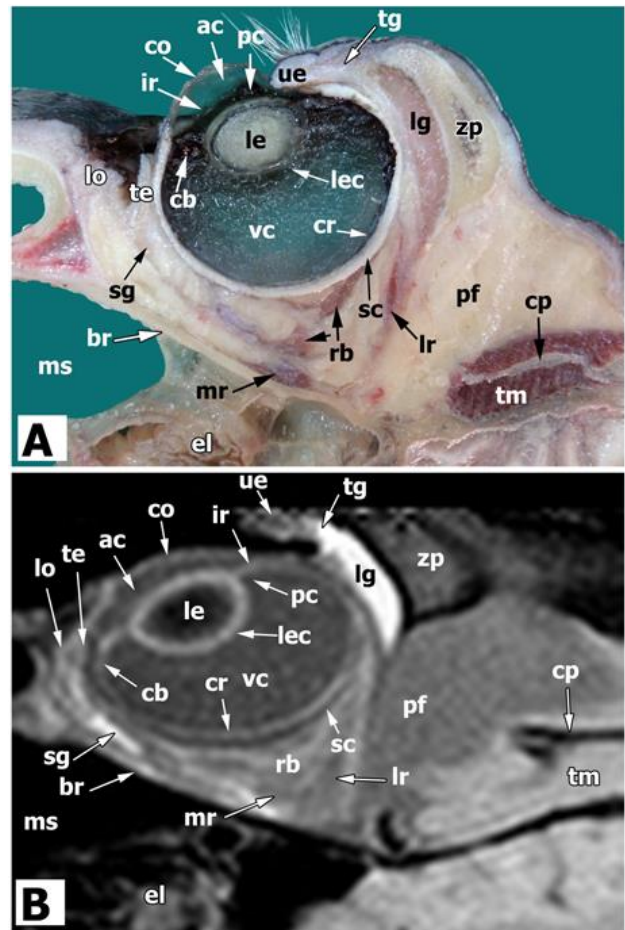


Fig. 5: Frontal sections of the left eye of the donkey (plane 4 as designated in Figure 1): anatomical section (A) and T1-weighted magnetic resonance image (B). ac- anterior chamber, br- bony rim, cb- ciliary body, co- cornea, cp- coronoid process of the mandible, cr- choroid, el- ethmoidal labyrinth, ir- iris, le- lens, lec- lens capsule, lg- lacrimal gland, lo- lower eyelid, lr- lateral rectus muscle, mr- medial rectus muscle, ms- maxillary sinus, pc- posterior chamber, pf- orbital fat, rb- retractor bulbi muscle, sc- sclera, sg- superficial gland of the third eyelid, te- third eyelid, tg- tarsal gland, tm- temporal muscle, ue- upper eyelid, vc- vitreous chamber, zp- zygomatic process of frontal bone.

complex which was outlined on T1-weighted images as hypointense structure (Figs. 7, 8/msc) and hyperintense on T2-weighted MR images (Fig. 4/msc). Both right and left optic nerves ran caudally within the corresponding optic canals as intracanalicular part (Fig. 8/onc). The meningeal sheath surrounding the intracanalicular part couldn't be outlined. The intracranial part (Fig. 8/onr) continued caudally to be decussated in the optic chiasma which appeared hyperintense on T1-weighted images (Fig. 8/oc). The other nerves and blood vessels supplying the eye globe couldn't be visualized on MR images or dissected sections.

DISCUSSION

The compared magnetic resonance images and gross sections used in this study provided a precise anatomical reference of the orbit, retrobulbar structures and optic nerve. This anatomic reference could help the clinicians to evaluate many ocular diseases. In addition, the given data could assist in establishing a functional anatomical reference of the ophthalmology in the donkey using MRI.

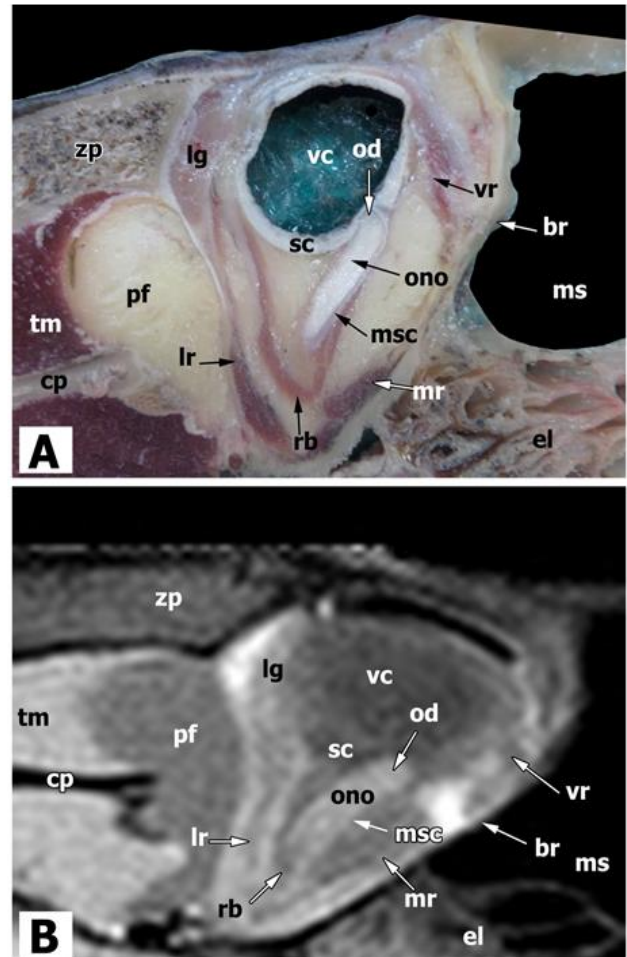
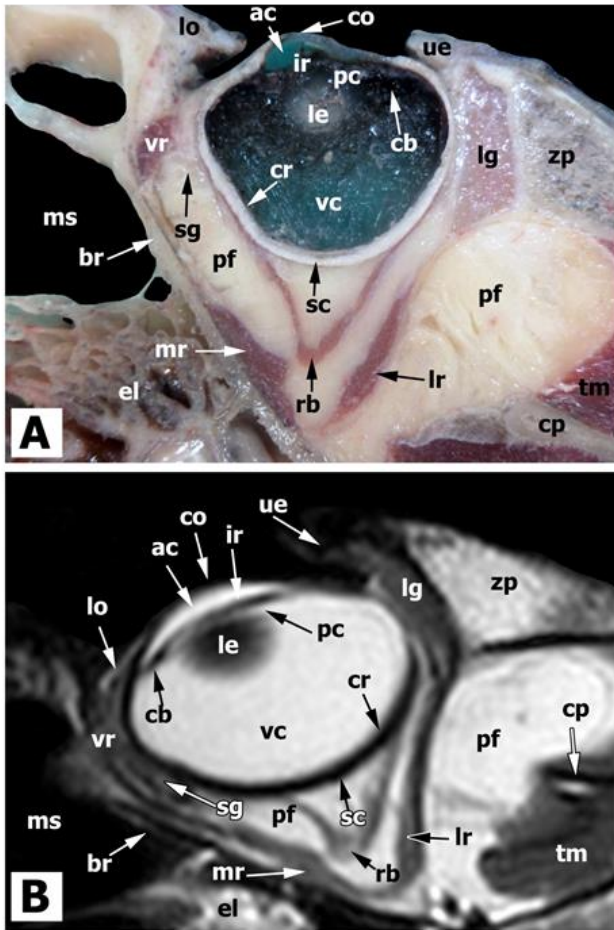


Fig. 6: Frontal sections of the right eye of the donkey (plane 5 as designated in Figure 1): anatomical section (A) and T2-weighted magnetic resonance image (B). ac- anterior chamber, br- bony rim, cb- ciliary body, co- cornea, cp- coronoid process of the mandible, cr- choroid, el- ethmoidal labyrinth, fs- frontal sinus, ir- iris, lg- lacrimal gland, lo- lower eyelid, lr- lateral rectus muscle, mr- medial rectus muscle, ms- maxillary sinus, pc- posterior chamber, pf- orbital fat, rb- retractor bulbi muscle, sc- sclera, sg- superficial gland of the third eyelid, tm- temporal muscle, ue- upper eyelid, vc- vitreous chamber, vr- ventral rectus muscle, zp- zygomatic process of frontal bone.

Fig. 7: Frontal sections of the left eye of the donkey (plane 6 as designated in Figure 1): anatomical section (A) and T1-weighted magnetic resonance image (B). br- bony rim, cp- coronoid process of the mandible, el- ethmoidal labyrinth, lg- lacrimal gland, lr- lateral rectus muscle, mr- medial rectus muscle, ms- maxillary sinus, msc- meningeal sheath complex, od- optic disc, ono- intraorbital part of the optic nerve, pf- orbital fat, rb- retractor bulbi muscle, sc- sclera, tm- temporal muscle, vc- vitreous chamber, vr- ventral rectus muscle, zp- zygomatic process of the frontal bone.

Using high resolution multi-planar MRI in this study admitted better visualization and overall orientation of the ocular structures, orbital cavity, orbital relationships, fluid chambers, retrobulbar structures, the optic nerve (intracranial extension) and optic chiasma. Recognition of these anatomical features is helpful for early detection and interpretation of the ophthalmic diseases and their intracranial extension (Kono et al. 2002; Aviv and Casselman 2005), as well as during application of the orbital diagnostic devices to avoid traumatic injuries (Michau and Gilger 2004).

In the current investigation, MRI admitted a good depiction of the neighboring paranasal sinuses to the orbital cavity. This topographic relationship might help in the extension of the infection to the orbit, as about 60% of the human ocular diseases are caused by bacterial infections which mostly originated from the paranasal sinuses (Rootman 2002). So, clinical studies explaining the origin and extension of the orbital diseases are recommended.

In accordance with Weber et al. (1996), Smith and Strotzman (2001) and Casselman et al. (2008), the optic

nerve pathway could be classified into intraocular, intraorbital, intracanalicular and intracranial parts. In addition, the optic nerve in the study under investigation could be differentiated from its surrounding meningeal sheath using MRI which could help to distinguish between the affections of the meningeal sheath and those of the nerve (Hickman et al. 2005; Goh et al. 2008). Meanwhile, the meningeal sheath around the intracanalicular part of the optic nerve couldn't be delineated in our study, which might be attributed to the close contact of the meningeal sheath to the bony optic canal (Boroffka et al. 2008). This discrimination between the nerve under investigation and its sheath complex can't be outlined using CT (Ettl et al. 2000).

The current investigation provided high contrast images of both chambers of the eye using MRI. However, the posterior chamber of the eye globe was small-sized to be outlined using ultrasonography (Rogers et al. 1986). Furthermore, Using MRI in this study permitted a clear depiction of the bony rim and deep cavity of the orbit, which could enable a full assessment of the process of bony invasion/lysis (Davis et al. 2002; Goh et al. 2008).



Fig. 8: Frontal T1-weighted MR image showing the pathway of the optic nerve in the donkey. cp- coronoid process of the mandible, el- ethmoidal labyrinth, msc- meningeal sheath complex, oc- optic chiasma, onc- Intracanalicular part of the optic nerve, ono- intraorbital part of the optic nerve, onr- intracranial part of the optic nerve, pf- orbital fat, tm- temporal muscle, vc- vitreous chamber.

While ultrasonography can't be used for evaluation of the bony involvement in the ocular pathological processes due to its limited visualization of the bony structures (Wilke and Gilger 1998).

Similar to the observations of Aviv and Casselman (2005), Goh et al. (2008) and D'Aout et al. (2014), our results reported that the retina couldn't be visualized using MRI. On the other hand, the choroid was clearly delineated from the sclera using MRI in the present investigation, this comes in disagreement with the findings of Reef (1998), Wilke and Gilger (1998) and D'Aout et al. (2014).

Regarding the periorbital structures, they could be depicted and outlined using MRI in this study including the glands (lacrimal, tarsal, superficial gland of the third eyelid), eyelids (upper, lower and third), extraocular muscles and orbital fat. On contrary, poor details for the periorbital structure could be observed using ultrasonography (Williams and Wilkie 1996; Penninck et al. 2001; Bentley et al. 2003), while the superficial gland of the third eyelid can't be visualized in the previous MRI studies in equine (D'Aout et al. 2014).

Conclusion

The present study provided a detailed anatomic description of the eyeball together with the optic nerve using MRI which could help in the future diagnosis and choice of the most appropriate surgery of the ocular diseases in the donkey.

Acknowledgement

The authors would like to thank all radiology team, El-Eman Scan Radiology Center, Beni-Suef Governorate, for performing MRI scanning.

Author's Contribution

Azza AH, Ibrahim, Mohamed KM, Abdel Maksoud collected literature of the manuscript then drafted it in consultation with Ashraf S. Awaad, while the MRI reading

was done by Fatma M. Halfaya. All authors approved the final manuscript.

REFERENCES

- Abdel Maksoud MKM, 2020. Normal anatomic reference of pastern and coffin joints in Egyptian buffalo *Bubalus bubalis*: A compared atlas of cross-sectional anatomy, magnetic resonance imaging and computed tomography. *Anatomia Histologia Embryologia* 49: 290-298. <https://doi.org/10.1111/ah.12527>
- Abdel Maksoud MKM, 2021. Gross anatomical, computed tomographic and magnetic resonance imaging study of the metacarpo/metatarsophalangeal joint in Egyptian buffalo *Bubalus bubalis*. *Anatomia Histologia Embryologia* 50: 360-372. <https://doi.org/10.1111/ah.12637>
- Abdel Maksoud MKM, Halfaya FM, Mahmoud HH and Ibrahim AAH, 2021. Morphological characteristics of the forebrain in the donkey *Equus asinus*: A compared atlas of magnetic resonance imaging and cross-sectional anatomy. *Anatomia Histologia Embryologia* 50: 974-984 <https://doi.org/10.1111/ah.12744>
- Aironi VD and Gandage SG, 2009. Pictorial essay: B-scan ultrasonography in ocular abnormalities. *Indian Journal of Radiology and Imaging* 19: 109-115. <https://doi.org/10.4103/0971-3026.50827>
- Amin ME, Elbakary MAR, Alsafy AMM and Fathi N, 2014. Radiographic and computed tomographic anatomy of the fetlock, pastern and coffin joints of the manus of the donkey *Equus asinus*. *Alexandria Journal of Veterinary Sciences* 41: 68-79. <https://doi.org/10.5455/ajvs.156620>
- Armour MD, Broome M, Dell'Anna G, Blades NJ and Esson DW, 2011. A review of orbital and intracranial magnetic resonance imaging in 79 canine and 13 feline patients 2004–2010. *Veterinary Ophthalmology* 144: 215–226. <https://doi.org/10.1111/j.1463-5224.2010.00865.x>
- Athar H, Parrah JD, Mir AQ, Moulvi BA, Makhdoomi DM, Dar MU and Handoo N, 2021. Ocular Ultrasonography and Echobiometry in Goats of Different Age and Breed. *Indian Journal of Animal Research* B-4360: 1-5. <https://doi.org/10.18805/IJAR.B-4360>
- Aviv RI and Casselman J, 2005. Orbital imaging: Part 1. Normal anatomy. *Clinical Radiology* 60: 279-287. <https://doi.org/10.1016/j.crad.2004.05.017>
- Awaad AS, Abdel Maksoud MKM and Fathi MZ, 2019. Surgical anatomy of the nasal and paranasal sinuses in Egyptian native sheep *Ovis aries* using computed tomography and cross sectioning. *Anatomia Histologia Embryologia* 48: 279-289. <https://doi.org/10.1111/ah.12436>
- Bentley E, Miller PE and Diehl KA, 2003. Use of high-resolution ultrasound as a diagnostic tool in veterinary ophthalmology. *Journal of American Veterinary Medical Association* 223: 1617–1622. <https://doi.org/10.2460/javma.2003.223.1617>
- Boroffka SA and Voorhout G, 1999. Direct and reconstructed multiplanar computed tomography of the orbits of healthy dogs. *American Journal of Veterinary Research* 60: 1500-1507.
- Boroffka SA, Verbruggen AM, Grinwis GC, Voorhout G and Barthez PY, 2007. Assessment of ultrasonography and computed tomography for the evaluation of unilateral orbital disease in dogs. *Journal of the American Veterinary Medical Association* 230: 671–680. <https://doi.org/10.2460/javma.230.5.671>
- Boroffka SAEB, Gorig C, Auriemma E, Passon-Vastenburger MHAC, Voorhout G and Barthez PY, 2008. Magnetic resonance imaging of the canine optic nerve. *Veterinary Radiology and Ultrasound* 49: 540-544. <https://doi.org/10.1111/j.1740-8261.2008.00427.x>
- Casselman J, Mermuys K, Delanote J, Ghekiere J and Coenegrachts K, 2008. MRI of the cranial nerves-more than meets the eye: technical considerations and advanced anatomy. *Neuroimaging Clinics of North America* 182: 197-231. <https://doi.org/10.1016/j.nic.2008.02.002>

- D'Aout C, Nisolle JF, Navez M, Perrin R, Launois T, Brogniez L, Clegg P, Vandeweerd JM and Hontoir F, 2014. Computed tomography and magnetic resonance anatomy of the normal orbit and eye of the horse. *Anatomia Histologia Embryologia* 445: 370-377. <https://doi.org/10.1111/ah.12149>
- Davis JL, Gilger BC, Spaulding K, Robertson ID and Jones SL, 2002. Nasal adenocarcinoma with diffuse metastases involving the orbit, cerebrum, and multiple cranial nerves in a horse. *Journal of American Veterinary Medical Association* 221: 1460-1463. <https://doi.org/10.2460/javma.2002.221.1460>
- Dennis R, 2000. Use of magnetic resonance imaging for the investigation of orbital disease in small animals. *Journal of Small Animal Practice* 41: 145-155. <https://doi.org/10.1111/j.1748-5827.2000.tb03184.x>
- Ettl AR, Zwrtek K, Daxer A and Salomonowitz E, 2000. Anatomy of the orbital apex and cavernous sinus on high resolution magnetic resonance images. *Survey of Ophthalmology* 44: 303-323. <https://doi.org/10.1016/s0039-62579900115-0>
- Evans, HE and de Lahunta A, 2013. *Miller's anatomy of the dog*. 4th Ed. Philadelphia: Elsevier Saunders, pp: 790-710.
- FAO Food and Agriculture Organization of the United Nations 2009. Retrieved from <http://www.fao.org/get-involved/ask-fao/en>
- Gialletti R, Marchegiani A, Valeriani T, Nannarone S, Beccati F, Fruganti A and Laus F, 2018. A survey of ocular ultrasound abnormalities in horse: 145 cases. *Journal of Ultrasound* 211: 53-59. <http://doi.org/10.1007/s40477-018-0284-7>
- Goh PS, Gi MT, Charlton A, Tan C, Gangadhara Sundar JK and Amrith S, 2008. Review of orbital imaging. *European Journal of Radiology* 66: 387-395. <http://doi.org/10.1016/j.ejrad.2008.03.031>
- Grahn BH, Stewart WA, Towner RA and Noseworthy MD, 1993. Magnetic resonance imaging of the canine and feline eye, orbit, and optic nerves and its clinical application. *Canadian Veterinary Journal* 34: 418-424 <https://pubmed.ncbi.nlm.nih.gov/17424252/>
- Hande PC and Talwar I, 2012. Multimodality imaging of the orbit. *Indian Journal of Radiology and Imaging* 223: 272-239. <https://doi.org/10.4103/0971-3026.107184>
- Hallowell GD and Bowen IM, 2007. Practical ultrasonography of the equine eye. *Equine Veterinary Education* 1911: 600-605. <https://doi.org/10.2746/095777307X254536>
- Hickman SJ, Miszkiel KA, Plant GT and Miller DH, 2005. The optic nerve sheath on MRI in acute optic neuritis. *Neuroradiology* 47: 51-55. <https://doi.org/10.1007/s00234-004-1308-x>
- Kato K, Nishimura R, Sasaki N, Matsunaga S, Mochizuki M, Nakayama H and Ogawa H, 2005. Magnetic resonance imaging of a canine eye with melanoma. *Journal of Veterinary Medical Science* 672: 179-182. <https://doi.org/10.1292/jvms.67.179>
- Konig HE and Liebich HG, 2009. *Veterinary anatomy of domestic mammals*. 3rd Ed. Scattauer GmbH, Stuttgart, Germany, pp: 547-567.
- Kono R, Poukens V and Demer JL, 2002. Quantitative analysis of the structure of the human extraocular muscle pulley system. *Investigative Ophthalmology and Visual Science* 43: 2923-2932. <https://pubmed.ncbi.nlm.nih.gov/12202511/>
- Laus F, Paggi E, Marchegiani A, Cerquetella M, Spaziante D, Faillace V and Tesi B, 2014. Ultrasonographic biometry of the eyes of healthy adult donkeys. *Veterinary Record* 174: 326-328. <https://doi.org/10.1136/vr.101436>
- Litwiller DV, Lee SJ, Kolipaka A, Mariappan YK, Glaser KJ, Pulido JS and Ehman RL, 2010. Magnetic resonance elastography of the ex-vivo bovine globe. *Journal of Magnetic Resonance Imaging* 321: 44-51. <https://doi.org/10.1002/jmri.22217>
- Madkour N, Amin M, Karkoura AA, Alsafy MAM and El-Gendy SA, 2016. Computed tomography and gross anatomical studies of the orbital cavity of the baladi goat (*Capra hircus*). *Alexandria Journal of Veterinary Sciences* 512: 74-81. <https://doi.org/10.5455/ajvs.245815>
- Mafee MF, 2003. Orbit: Embryology, anatomy and pathology. In: *Head and Neck Imaging*. Som PM, Curtin HD eds. 4 Ed. vol. 2. St Louis: Mosby, pp: 534-6.
- Maiolo C, Fresina M and Campos EC, 2017. Role of magnetic resonance imaging in heavy eye syndrome. *Eye* 31: 1163-1167. <https://doi.org/10.1038/eye.2017.48>
- Michau TM and Gilger BC, 2004. Cosmetic globe surgery in the horse. *Veterinary Clinics of North America: Equine Practice* 20: 467-484. <https://doi.org/10.1016/j.cveq.2004.04.001>
- Morgan RV, Daniel GB and Donnell GB, 1993. Magnetic resonance imaging of the normal eye and orbit of the horse. *Progress in Veterinary & Comparative Ophthalmology* 3: 127-133.
- Morgan RV, Daniel BD and Donnell L, 1994. Magnetic resonance imaging of the normal eye and orbit of the dog and cat. *Veterinary Radiology & Ultrasound* 35: 102-108. <https://doi.org/10.1111/j.1740-8261.1994.tb00196.x>
- Nell B, 2008. Optic neuritis in dogs and cats. *Veterinary Clinics of North America: Small Animal Practice* 38: 403-415. <https://doi.org/10.1016/j.cvsm.2007.11.005>
- Nomina Anatomica Veterinaria, 2017. International Committee on Veterinary Gross Anatomical Nomenclature and authorized by the general assembly of the World Association of Veterinary Anatomist. 6th Ed. Published by the Editorial Committee Hanover Germany, Ghent Belgium.
- Penninck D, Daniel GB, Brawer R and Tidwell AS, 2001. Cross-sectional imaging techniques in veterinary ophthalmology. *Clinical Techniques in Small Animal Practice* 16: 22-39. <https://doi.org/10.1053/svms.2001.22802>
- Reef VB, 1998. Ultrasonographic evaluation of small parts. In: *Equine diagnostic ultrasound*. Reef VB ed, Philadelphia: WB Saunders, pp: 480-547.
- Rogers M, Cartee RE, Miller W and Ibrahim AK, 1986. Evaluation of the extirpated equine eye using B-mode ultrasonography. *Veterinary Radiology* 27: 24-29.
- Rootman J, 2002. Distribution and differential diagnosis of orbital disease. In: *Diseases of the orbit: A multidisciplinary approach*. 2nd Ed. Philadelphia, PA: Lippincott, Williams and Wilkins, pp: 52-84.
- Salavati S, Karimi S and Khafi MSA, 2017. Ocular Ultrasonographic Features in Iranian Native Donkey. *Iranian Journal of Veterinary Surgery* 112: 15-19.
- Seddek AM, Abedallaah BA and Awaad AS, 2014. Computed tomography and dissection anatomy of the frontal and maxillary sinuses in native Egyptian goats. *Indian Journal of Veterinary Surgery* 351: 12-16.
- Smith MM and Strotzman JM, 2001. Imaging of the optic nerve and visual pathways. *Seminars in Ultrasound, CT, and MRI*, 226: 473-487. <https://doi.org/10.1016/s0887-21710190002-2>
- Solano M and Brawer RS, 2004. CT of equine head: Technical consideration, anatomical guide, and selected disease. *Clinical Techniques in Equine Practice* 3: 364-388. <https://doi.org/10.1053/j.ctep.2005.02.016>
- Thrall DE, 2013. *Textbook of veterinary diagnostic radiology*. 6th Ed. Elsevier Saunders, Missouri: USA, pp: 50-55.
- Van der Woerd A, 2008. Orbital inflammatory disease and pseudotumor in dogs and cats. *Veterinary Clinics of North America: Small Animal Practice* 38: 389-401. <https://doi.org/10.1016/j.cvsm.2007.11.006>
- Weber AL, Klufas R and Pless M, 1996. Imaging evaluation of the optic nerve and visual pathway including cranial nerves affecting the visual pathway. *Neuroimaging Clinics of North America* 6: 143-177.
- Williams J and Wilkie D, 1996. Ultrasonography of the eye. *Compendium on Continuing Education for the Practicing Veterinarian* 18: 667-677.
- Wilke DA and Gilger BC, 1998. Equine diagnostic ocular ultrasonography. In: *Equine diagnostic ultrasound*. Reef VB ed, Philadelphia: WB Saunders, pp: 637-645.